*Acta Oceanol. Sin.*, 2016, Vol. 35, No. 5, P. 9–17
DOI: 10.1007/s13131-015-0741-5
http://www.hyxb.org.cn
E-mail: hyxbe@263.net

# The decadally modulating eddy field in the upstream Kuroshio Extension and its related mechanisms

WANG Shihong[1, 2], LIU Zhiliang[1]*, PANG Chongguang[1], LIU Huiqing[3]

[1] Key Laboratory of Ocean Circulation and Waves, Institute of Oceanology, Chinese Academy of Sciences, Qingdao 266071, China

[2] College of Earth Science, University of Chinese Academy of Sciences, Beijing 100049, China

[3] International Hurricane Research Center, Florida International University, Miami, MARC 370, USA

Received 12 May 2015; accepted 6 September 2015



**Abstract**

Both the level of the high-frequency eddy kinetic energy (HF-EKE) and the energy-containing scale in the upstream Kuroshio Extension (KE) undergo a well-defined decadal modulation, which correlates well with the decadal KE path variability. The HF-EKE level and the energy-containing scales will increase with unstable KE path and decrease with stable KE path. Also the mesoscale eddies are a little meridionally elongated in the stable state, while they are much zonally elongated in the unstable state. The local baroclinic instability and the barotropic instability associated with the decadal modulation of HF-EKE have been investigated. The results show that the baroclinic instability is stronger in the stable state than that in the unstable state, with a shorter characteristic temporal scale and a larger characteristic spatial scale. Meanwhile, the regional-averaged barotropic conversion rate is larger in the unstable state than that in the stable state. The results also demonstrate that the baroclinic instability is not the dominant mechanism influencing the decadal modulation of the mesoscale eddy field, while the barotropic instability makes a positive contribution to the decadal modulation.

**Key words:** Kuroshio Extension, mesoscale eddy, decadal modulation, baroclinic instability, barotropic energy conversion rate, nonlinear eddy-eddy interaction

**Citation:** Wang Shihong, Liu Zhiliang, Pang Chongguang, Liu Huiqing. 2016. The decadally modulating eddy field in the upstream Kuroshio Extension and its related mechanisms. Acta Oceanologica Sinica, 35(5): 9–17, doi: 10.1007/s13131-015-0741-5

## 1 Introduction

The Kuroshio Extension (KE) is an eastward-flowing current in the subtropical western North Pacific after the Kuroshio separates from the coast of Japan at 35°N, 140°E. Being the extension of a wind-driven western boundary current, the KE is rich in large-amplitude meanders and energetic eddies (Qiu, 2002). The KE region has the largest sea surface height (SSH) variability in the extratropical North Pacific, and also has the highest eddy kinetic energy (EKE) level (Qiu, 2002; Qiu and Chen, 2010). The occurrence and evolution of eddies play an important role in determining the surface ocean heat budget and winds at the overlying atmospheric boundary layer in this region (Qiu and Kelly, 1993; Vivier et al., 2002; Nonaka and Xie, 2003). They have a strong influence on the formation of the Subtropical Mode Water as well (Qiu and Chen, 2006).

There are a lot of papers in which KE system is studied by using the high-quality SSH measurements from the satellite altimeters. Many of them (e.g., Qiu and Chen, 2005, 2010; Bessières et al., 2013) have already detected a well-defined decadal modulation of the KE system including the KE jet, the southern recirculation gyre and their associated mesoscale eddy signals. This modulation consists of two rather different states (see Figs 3 and 4 in Bessières et al., 2013): a stable state corresponding to a narrow strong steady jet and an unstable state with a wider weaker jet. During stable periods, two quasi-stationary meanders well develop, and the mean latitudinal position of the KE jet is moving northward. The meanders are barely discernible during the unstable periods and the KE jet is moving southward. Simultaneously, the regional EKE level will increase when the system is stable, and decrease when the system is unstable (e.g., Qiu and Chen, 2010).

Considering the significant role of the KE in the North Pacific, it is important to investigate the mechanisms for the decadal variability. Qiu and Chen (2005, 2010) have done some valuable studies in this topic by using the accumulated high-quality satellite altimeter data. They pointed out that the transitions between the two states were caused by the basin-scale wind-stress curl forcing in the eastern North Pacific through the linear baroclinic Rossby wave, which was closely related to the Pacific decadal oscillation (PDO). During the positive PDO, the negative SSH anomalies in the eastern Pacific Ocean would propagate to the west as linear baroclinic wave, then they waken the zonal KE jet and the KE path is moving southward. On the other hand, during the negative PDO, it was completely reversed. The decadally modulating KE system is full of high nonlinear phenomena, such as the interactions of the recirculation, potential vorticity (PV) advection and eddies (Taguchi et al., 2007). Moreover, Pierini (2006) identified a mean meandering path and a decadal variability of

Foundation item: The National Natural Science Foundation of China under contract No. 41276026; the Special Fund for Strategic Pilot Technology Chinese Academy of Sciences under contract No. XDA11020301; the Joint Fund between Natural Science Foundation of China and Shandong Province under contract No. U1406401.

*Corresponding author, E-mail: zhlliu@qdio.ac.cn

the KE jet by using a reduced-gravity primitive equation ocean model with a time-independent climatological wind. The model results have a good agreement with *in situ* and altimetry measurements and indicate that the intrinsic nonlinear mechanisms are likely to play a major role in determining the meander pattern of the mean flow. Dijkstra and Ghil (2005) also got the similar conclusions from their studies. Taguchi et al. (2007) reconciled above two views through an empirical orthogonal function (EOF) analysis. Their results showed the nonlinear ocean dynamics still played an essential role in determining the spatial structure of the KE jet, while the linear Rossby wave theory could be used to explain the temporal variability.

Despite a gradual increase of our knowledge on the decadal variation of the KE system, it is still unclear that what are the dominant mechanisms influencing the decadal modulating mesoscale eddy field. The regional HF-EKE level tends to be low (high) at the strong (weak) KE jet state, which is rather counterintuitive. Since the jet instability analysis usually suggests that the stable stronger flows would favor linear baroclinic instabilites (Pedlosky, 1964), and lead to more mesoscale activities. If so, the baroclinic instability would not be the dominant mechanism influencing the decadal modulation of the mesoscale eddy field. However, the approximate agreement between linear theory and observations supports the view that the baroclinic instability is the main energy source of the geostrophic eddy field outside the tropical band (Ferrari and Wunsch, 2008). Therefore it is an interesting and useful topic to study the different role of the baroclinic instability in two different states. In this study, the local linear baroclinic instability is analyzed in both states, to quantitatively examine the extent that the linear baroclinic instability can explain the variability of the decadal modulation of the mesoscale eddy field.

The dynamics that give rise to the ocean eddy field are more complex than which is described by the linear theory alone. Moreover, the local approximation of linear baroclinic instability calculation ignores the eddy feedback on the mean flow under the steady assumption (Tulloch et al., 2011). Therefore we estimated quantitatively how much kinetic energy that the mesoscale eddy field extracts from the mean flow in different states, by calculating the barotropic energy conversion rate between the eddy field and the mean flow.

Furthermore, the development of mesoscale eddy field is not a linear process, but a turbulent process by which many scales are excited (e.g., Arbic and Flierl, 2004; Smith, 2007). It is also important to clarify the interactions between the mesoscale eddies, which determine a statistical stable spectral kinetic energy density of the real ocean. One effective diagnostic tool to assess the nonlinear eddy-eddy interaction is the scale-by-scale energy flux analysis advocated by Frisch (1995). This method was applied by Scott and Wang (2005) to reveal a baroclinic inverse kinetic energy cascade in the South Pacific Ocean from satellite altimetry measurements. In order to further understand the decadal modulating mesoscale eddy field, in this study, we have calculated the spectral kinetic energy flux in the upstream KE region to explore the differences of the mesoscale eddy nonlinear evolution in different states.

The paper is organized as follows. Section 2 describes datasets used in this study. In Section 3, we demonstrate the major results of the study. A summary and some discussions are shown in Section 4.

## 2 Data

### 2.1 *SSH and SSH anomaly*

Updated gridded SSH and SSH anomaly (SSHA) data used in this analysis were produced by Segment Sol Multimissions d'Alimétrie, d'Orbitographie et de Localization Precise/Data Unification and Altimeter Combination System (SSALTO/DUACS) and distributed by Archiving, Validation and Interpretation of Satellite Oceanographic Data (AVISO), with support from the Center National d'Etudes Spatiales (CNES). This dataset merges measurements from all available altimeter missions at a given time, including Jason-1, Jason-2, TOPEX/Poseidon, Envisat, Geosat Follow-On (GFO), European Remote Sensing Satellite (ERS) 1/2. So it has the best possible sampling and provides improved estimation of mesoscale signals (Le Traon et al., 1998, 2001; Ducet et al., 2000). See SSALTO/DUACS User Handbook for more details about the product generation. The maps have a 7-day temporal resolution, a 1/3-longitude Mercator spatial resolution, and cover the period from October 1992 through December 2014.

### 2.2 *Gridded temperature and salinity data based on ARGO Data*

In this study, we have also used the Version 4 of the Met Office Hadley Centre "EN" series of datasets, which is a global gridded NetCDF objective analyses of ocean potential temperature and salinity profiles obtained across the global oceans. The EN4 dataset is an incremental development of the previous versions EN2 and EN3, which was documented in Ingleby and Huddleston (2007) and at http://www.metoffice.gov.uk/hadobs/en3/. Data from all types of ocean profiling instruments that provide temperature and salinity information are ingested into the EN4 data set, including the latest version of the World Ocean Database (WOD09), data from the Global Temperature and Salinity Profile Program (GTSPP) and ARGO Data from 2000 onward. The EN4 data set has a regular 1° horizontal grid and 42 vertical levels and covers the period from 1900 to present. In this paper, we use the data set from the year 2000 to 2014, because it contains the ARGO Data and covers a full cycle of the decadal modulation of the KE.

## 3 Results

### 3.1 *Decadally modulating mesoscale eddy field in the upstream KE region*

One important feature increasing clearly from the long, available SSHA time series is that the level of high-frequency (HF) EKE (<300 d) in the upstream KE region undergoes a well-defined decadal modulation. It was noted in Qiu and Chen (2005) and Bessières et al. (2013) to be a manifestation of the decadal variability of the KE system. Figure 1a shows the time series of the HF-EKE averaged in the upstream KE region 30°–39°N, 142°–156°E. The HF-EKE is derived from the 300-day high pass filtered SSHA to extract the mesoscale from the lower frequency signals. The HF-EKE is then centered and filtered with a 55-week moving average to remove the seasonal signals. While the interannual variability also exists, the HF-EKE level in Fig. 1a clearly undergoes a decadal modulation. Compared to the mean HF-EKE level, 506 $cm^2/s^2$, the decadal HF-EKE modulation has a peak-to-peak amplitude of ~300 $cm^2/s^2$. The decadal variation has two complete cycles since 1993 and currently into the third cycle.

The KE system contains various types of mesoscale signals, including Rossby waves and turbulent eddies, such as meanderings, energetic pinched-off rings and isolated eddies. These mesoscale signals have different characteristic spatial scales and different characteristic temporal scales. This indicates that these signals are generated by different mechanisms, such as instabilit-

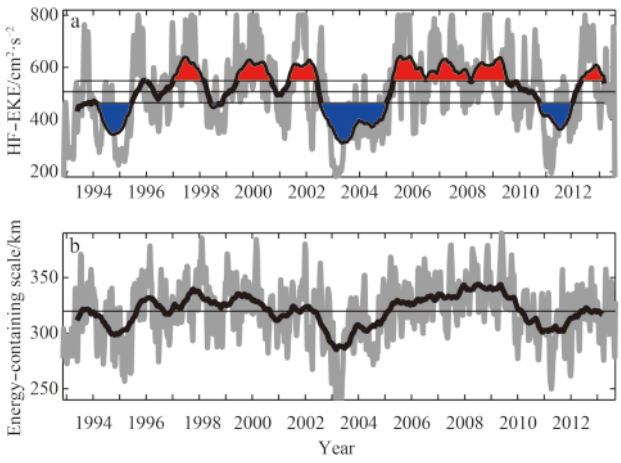


**Fig. 1.** Time series of the high frequency eddy kinetic energy (HF-EKE) in the upstream KE region (30°–39°N, 142°–156°E) (a) and energy-containing scale estimated from Eq. (1) (b). Blue shaded areas correspond to stable state periods, while red shaded areas fit unstable state periods. The black lines are the time series after a 55-week running mean is applied to the original weekly time series (gray lines).

ies, the eddy-mean flow interaction and excitation of Rossby waves (Tai and White, 1990; Waterman et al., 2011). To further explore the characters of the decadal modulating mesoscale eddy field in the upstream KE region, we have calculated the regional energy-containing length scale of HF-EKE, which is defined as

$$L_e(t) = 2\pi \sum_{k_x,\,k_y} E(k_x, k_y, t)\Delta k^2 / \sum_{k_x,k_y} K \cdot E(k_x, k_y, t)\Delta k^2, \quad (1)$$

where $K = \sqrt{k_x^2 + k_y^2}$ is the total wavenumber and $E(k_x, k_y, t)$ is HF-EKE power spectral density

$$E(k_x, k_y, t) \equiv \frac{1}{2}(\hat{u}\hat{u}^* + \hat{v}\hat{v}^*), \quad (2)$$

with the caret indicates discrete Fourier transform (DFT) and the star indicates complex conjugate. The time series of the energy-containing length scale $L_e$ has been shown in Fig. 1b. It is clear that $L_e$ experiences a very similar decadal modulations with the HF-EKE; the high (low) EKE level corresponds to the large (small) energy-containing scale. The linear correlation coefficient between the EKE and the energy-containing scale is about 0.60, and it increases to 0.85 when the seasonal signals are removed by 55-week moving average. The increase of the correlation is probably because the lag in $L_e$ behind the EKE (about 2–3 months) is not significant when the seaso nal variation is removed by smoothing. The lag has been demonstrated by Kobashi and Kawamura (2002) and Qiu et al. (2008) in the Subtropical Countercurrent (STCC).

Figure 1 shows that the KE system is stable in 1994, 2002–2004 and 2011, while it is unstable in 1997–2001 and 2006–2008. Note that this is not a strict classification, because between these states the KE jet has many intermediate states of transition presenting either progressively wakening or strengthening trend. Moreover, there are short-lived stable periods in unstable periods. In the following analysis, we collaborate all the stable periods (blue shaded in Fig. 1a) and unstable periods (red shaded in Fig. 1a), respectively, to conduct datasets for each state.

To further clarify the characters of the mesoscale eddy field in the upstream KE region in different states, which may be helpful to explore its generation mechanism, we have calculated the averaged power spectral densities in two states, $\bar{E}(k_x, k_y, t)$, as a function of zonal and meridional wavenumber, $k_x$ and $k_y$. It is clear from Fig. 2 that the mesoscale eddies have a higher energy level at large $k_y$ than at large $k_x$, implying that the mesoscale eddies are more zonally than meridionally, elongated in the unstable state (left panel). Meanwhile, in the stable state (right panel), most of the energy appears at nearly equal $k_x$ and $k_y$ with a tiny shift to larger $k_x$, which implies that the mesoscale eddies in this state are almost homogeneous with a little meridionally elongated. Because the baroclinic instability preferentially generates meridionally elongated signals (Qiu et al., 2008; Tulloch et al., 2011), it is very likely that in unstable state, the nonlinear transfer via triad eddy interaction works more effectively to redistribute EKE into zonally elongated signals. We will verify this possibility in the following subsections.

### 3.2 *Local baroclinic growth rates and scales of maximum instability*

When the KE jet is weaker (corresponding to the unstable state), the HF-EKE level in the upstream KE region is higher. However, based on the theory of the baroclinic instability (Pedlosky, 1964), less mesoscale eddies might be expected in the unstable state because of reduced instability of the weaker jet. It in-

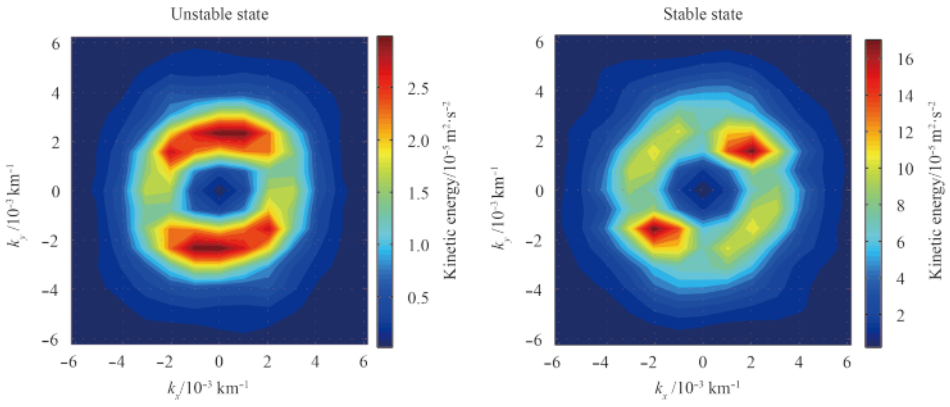


**Fig. 2.** Power spectral density distribution of HF-EKE as a function of $k_x$ and $k_y$ in the upstream KE region (30°–39°N, 142°–156°E).

dicates that the local baroclinic instability is not the dominant mechanism influencing the decadal modulation of the mesoscale eddy field in the upstream KE region. To examine this possibility quantitatively, we have diagnosed the characters of the local linear baroclinic instability, with focusing on the baroclinic growth rate and the scale of maximum instability.

Firstly, in Fig. 3 we have shown the neutral density structures in the 20°–40°N band, and across the KE system along 150°E in two states. The neutral density $\rho$ is computed from the average salinity and temperature field of the gridded ARGO dataset, analogously to Jackett and Mcdougall (1997). Then the mean geostrophic velocities $U(x,y,z)$, $V(x,y,z)$ are computed from density field $\bar{\rho}(x,y,z)$ through thermal wind balance:

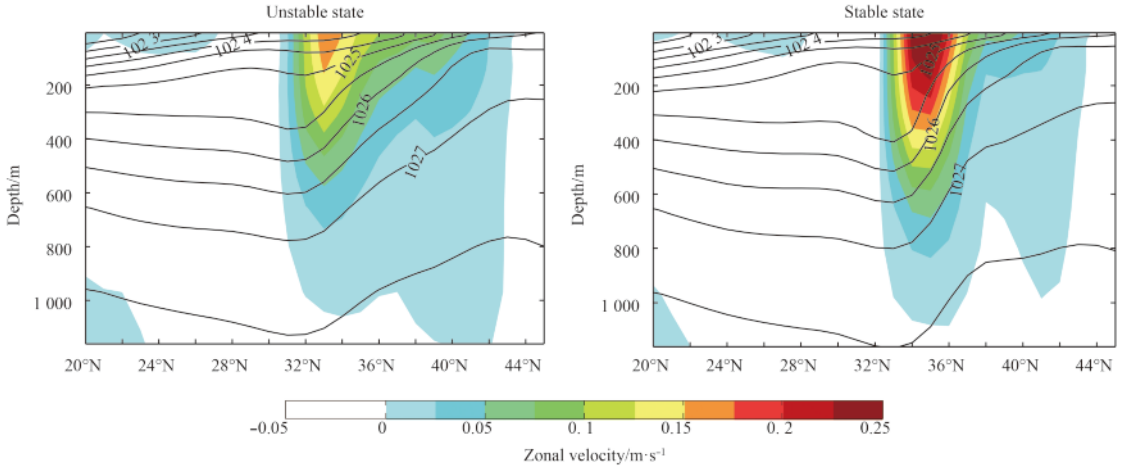


**Fig. 3.** Neutral density structures associated with the KE along 150°E in contours, and the contour units are kg/m$^3$; the mean geostrophic velocity field, shown in color (m/s), calculated from the neutral density through thermal wind principle.

$$f\frac{\partial}{\partial z}(-V,U)=\frac{g}{\rho_0}\nabla\bar{\rho}, \tag{3}$$

where $f$ is the Coriolis parameter and $\rho_0$ is the mean oceanic density. It is clear in Fig. 3 that the isopycnals have in general a downward slope toward the south in the 30°–40°N band of our interest. By comparing the thermohaline structures in different states, it is found that the isopycnals in the stable state are steeper than that in the unstable state. Simultaneously, the KE currents is weak in the unstable state, spreads on a wider latitudinal band, and the jet axis is at about 33°N. In the stable state, the KE currents is strong, gathers on a narrow latitudinal band, and the jet axis is at about 35°N. All these features of the KE currents are quite consistent with the altimeter observation (Qiu and Chen, 2005, 2010). This indicates that the gridded ARGO Data is able to capture the decadal variation of the KE system.

To demonstrate the likelihood of baroclinic instability, we have estimated an intrinsic eddy timescale by consideration of the energy conversion generated by baroclinic instability. It is derived by Smith (2007) by integrating the mean available potential energy (APE) $(f^2/2N^2)\Psi_z^2$ both vertically and horizontally over a box of length $L$, assuming a local mean streamfunction $\Psi(z)=-yU(z)+xV(z)$, to arrive at

$$\sigma=f\sqrt{\frac{1}{H}\int_{-H}^{0}\frac{\mathrm{d}z}{R(z)}}, \tag{4}$$

after neglecting the cross term. $R(z)=N^2/(U_z^2+V_z^2)$ is the Richardson number, $N^2(z)=-(g/\rho_0)\mathrm{d}\bar{\rho}/\mathrm{d}z$ represents the stratification, and $H$ is the vertical depth. As stated by Smith (2007) $\sigma\propto\sqrt{APE}$, where $APE\cong\frac{\rho_0 L^4}{6}\int_{-H}^{0}\frac{f^2}{R(z)}\mathrm{d}z$. Physically, $\sigma^{-1}$, known as Eady timescale (Eady, 1949), reflects the intrinsic strength of the baroclinic instability. A smaller value of the Eady timescale represents more of mean APE, and a higher growth rate of baroclinic instability, which indicates more (less) mesoscale signals might be expected. Figure 4 shows the Eady timescale in two states. Note that the upstream KE region gets a characteristic temporal scale about 10 d, which is substantially smaller than that in the adjacent southern and northern recirculation gyres in both states. It indicates that the KE region stores more of APE than its adjacent recirculation gyres. By contrasting, it is clear that the Eady time scale in the stable state is notably smaller than that in the unstable state (for about 5 d), which indicates the thermohaline structure of KE stores more of mean APE in the stable state than in the unstable states.

We have also estimated the characteristic scales of maximum baroclinic instability in the upstream KE region to keep a self-contained system of the local linear baroclinic analysis. Characteristic eddy scales are computed by solving the linearized quasigeostrophic equations about the local climatological streamfunction $\Psi(z)=V(z)x-U(z)y$ and stratification $N^2(z)$.

$$\partial_t q+J(\Psi,q)+J(\psi,\beta y+\Gamma\Psi)=0,\quad -H<z<0, \tag{5}$$

$$\partial_t b+J(\Psi,b)+J(\psi,f\partial_z\Psi)=0,\quad z=-H,0, \tag{6}$$

where $\Gamma=\partial_z(f^2/N^2\partial_z)$ is the vortex stretching operator, $b=f\partial\psi/\partial z$ is the buoyancy, and $q=(\nabla^2+\Gamma)\psi$ is the QGPV. A form of wave solution $\psi=\Phi(z)\exp(i(k_x x+k_y y-\omega t))$ is assumed. At a given $K=k_x,k_y$, the eigenvalue $\omega$ is the corresponding wave frequency and its imaginary part produces the growth of the wave. $\omega$ with the largest imaginary part is defined as the baroclinic growth rate, and the reciprocal of the corresponding $K=\left(k_x^2+k_y^2\right)^{1/2}$ is defined as the wavenumber of the maximum

linear growth. Readers are directed to Tulloch et al. (Tulloch et al., 2009; Tulloch et al., 2011) and Wang et al. (2015) for calculation details. Figure 5 shows the detailed stability calculations at 150°E, 35°N in the two states. Each row of Fig. 5 shows the neutral density profile, geostrophic zonal (solid line) and meridional (dash line) current profiles, and growth rate as a function of $k_x$ and $k_y$. The differences of the neutral density between the two states are not very significant, while the geostrophic meridional velocity and patterns of the growth rate are largely different in different states. In the unstable state (upper panels), the fastest growth rate (black dots in the third column) is about 0.047 $d^{-1}$, so the temporal scale is about 21 d, and the corresponding spatial scale is 314 km ($K/K_{def} \approx 0.7$, and the average Rossby deformation scale $L_{def}$ is about 220 km in this region). In the stable state (lower panels), the fastest growth rate is about 0.075 $d^{-1}$, so the temporal scale is about 13 d, and the corresponding spatial scale is about 366 km ($K/K_{def} \approx 0.6$). The shorter characteristic temporal scale and the larger characteristic spatial scale in the stable state indicate that more mesoscale signals could be generated through the linear baroclinic instability.

### 3.3 *Barotropic energy conversion rate*

The baroclinic instability occurs in rotating, stratified fluids with strong vertical shear, and the EKE is extracted from the APE and stored in the density fronts, while the barotropic instability occurs in the presence of strong horizontal shear and transfers the kinetic energy of the mean flow to the eddy field. The barotropic instability dominates in the tropics where the EKE is dominated by seasonal oscillations of the equatorial currents in response to shifts in the intertropical convergence zone and its as-

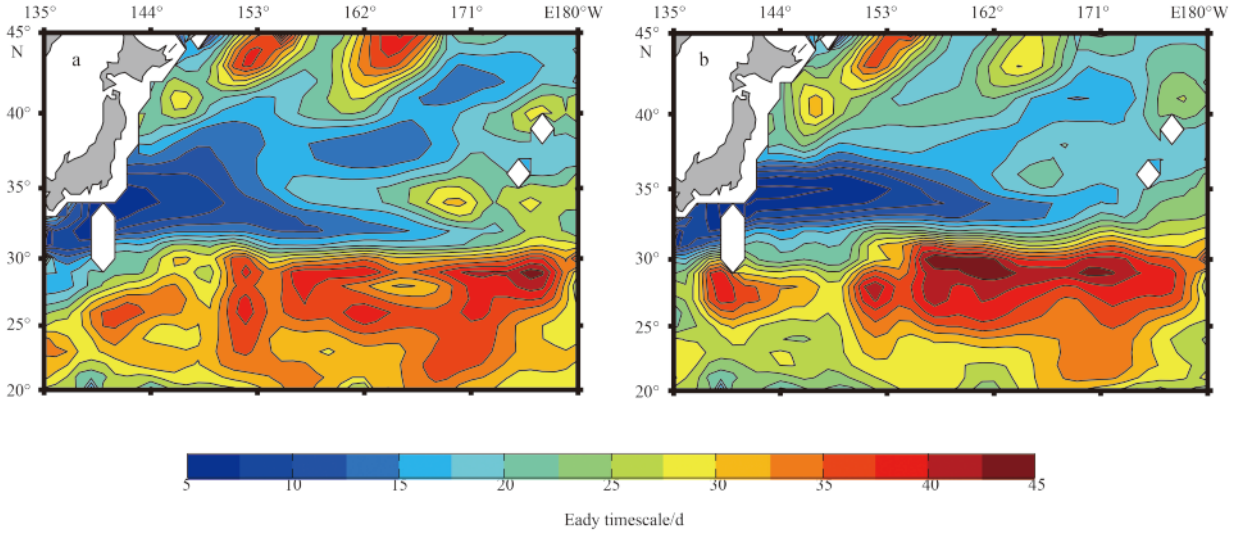


**Fig. 4.** Averaged spatial patterns of the Eady timescale (d) in unstable state (a) and stable state (b).

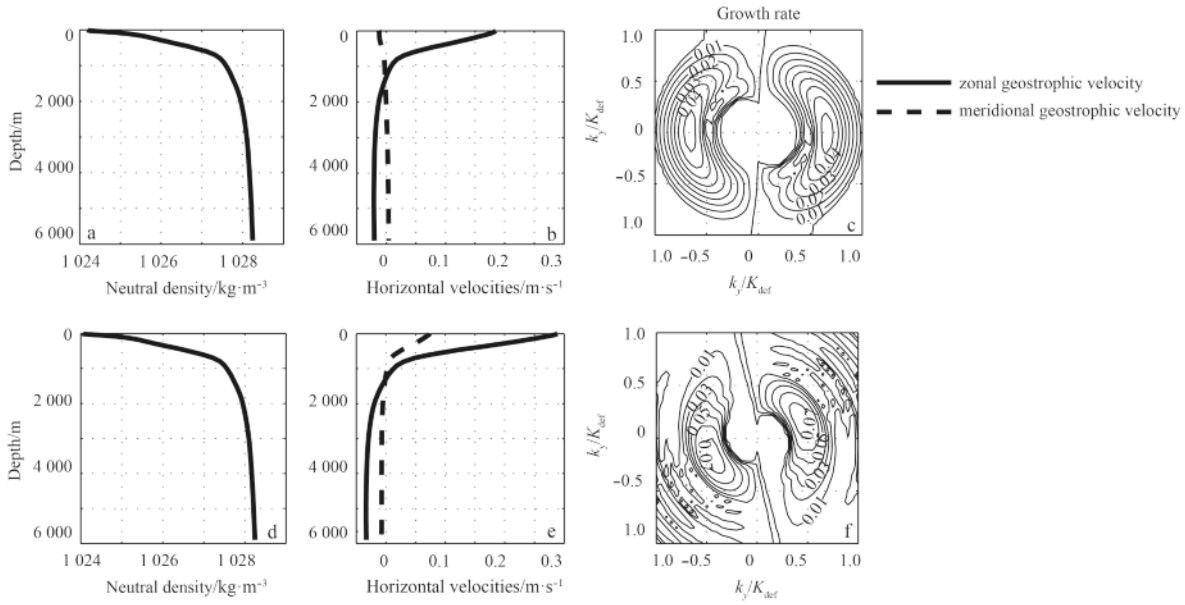


**Fig. 5.** Local baroclinic instability analysis at 35°N, 150°E in unstable state (a, b, c) and stable state (d, e, f).

sociated wind patterns (Ferrari and Wunsch, 2008). When the KE system is unstable, the path of KE currents migrates frequently. Intuitively, there might be more EKE extracted from kinetic energy of the mean flow through barotropic instabilities in the unstable state, which is analogous to that in tropics. Therefore, we have diagnosed the barotropic energy conversion rate in two different states to confirm, or refute this possibility.

The energy conversion rate between the time-mean flow and eddy field has been calculated by following the methods of Dewar and Bane (1989) and Berloff and Meacham (1998):

$$BT(x,y) = -\overline{u'_g u'_g}\frac{\overline{\partial u_g}}{\partial x} - \overline{u'_g v'_g}\left(\frac{\overline{\partial u_g}}{\partial y} + \frac{\overline{\partial v_g}}{\partial x}\right) - \overline{v'_g v'_g}\frac{\overline{\partial v_g}}{\partial y}, \quad (7)$$

where $\left(u'_g, v'_g\right) = \left(-\frac{g}{f}\frac{\partial SSHA}{\partial y}, \frac{g}{f}\frac{\partial SSHA}{\partial x}\right)$, and $(\overline{u_g}, \overline{v_g}) = \left(-\frac{g}{f}\frac{\partial SSH}{\partial y}, \frac{g}{f}\frac{\partial SSH}{\partial x}\right)$. According to Eq. (7), the barotropic energy conversion rate (BT) is proportional to the horizontal velocity shear. A positive BT value represents kinetic energy transfers from the mean flow to the eddy field, and vice versa.

Figure 6 shows spatial distributions of BT in the KE region in two states. It reveals that the energy conversion mainly occurs near to the KE jet in both states, with a conversion rate about $O\left(10^{-7}\,\mathrm{m^2/s^3}\right)$, while in regions far away from the jet it is about $O\left(10^{-8}\,\mathrm{m^2/s^3}\right)$. By comparing Fig. 6, it is found that the large BT spreads on a wider latitudinal band in the unstable state (left panel) than in the stable state. Meanwhile in the stable state, the large BT is more likely along the KE jet and the bimodal structure is clearly visible. A remarkable feature in the stable state is that, in front of a trough and back of a crest, kinetic energy transfers from the mean flow to the eddy field powerfully, while in front of a crest and back of a trough, kinetic energy transfers from eddy field to the mean flow. However, it is not significant in the unstable state, because of the frequent change of the jet path.

The mean BT (in the region with a gray rectangle domain containing 12 overlapping boxes in Fig. 6, which is identical to the region for HF-EKE calculation) is calculated to get straight comparison between the two states. The mean BT is 3.5×10$^{-8}$ m$^2$/s$^3$ in the stable state, and 4.7×10$^{-8}$ m$^2$/s$^3$ in the unstable state. The barotropic energy conversation rate is larger in the unstable state than that in the stable state. It is notable that the mean barotropic conversation rate is even larger in the unstable state, because the long-time averaged produces counteractions of the BT.

Strictly, one cannot isolate the barotropic instability and the baroclinic instability, as the necessary condition for instability of a flow with both horizontal and vertical shear is defined by the sign change of its total PV gradient (Phillips, 1954; Charney and Stern, 1962). Nevertheless, above calculations of both baroclinic and barotropic growth rate provide heuristic values in considering the potential barotropic and baroclinic instability independently, to gain insight into the relative contributions of horizontal and vertical shears to the EKE.

### 3.4 *Nonlinear eddy-eddy interaction*

It is well-known that the development process of ocean eddies is not a linear process, but a turbulent process by which many scales are excited. To a great extent, clarifying the interaction of the mesoscale eddies is of equal importance to knowing their generation mechanisms, since the processes determine the equilibrium geographic turbulent state of the world's oceans and might be helpful to understand the decadal modulation of the upstream KE mesoscale eddy field. We have made use of the approach of Scott and Wang (2005) to assess the nonlinear eddy-eddy interaction by calculating the spectral kinetic energy flux in wavenumber space, which is defined as

$$\Pi_K = \langle \mathrm{u}_K^< \cdot (\mathrm{u}_K^< \cdot \nabla \mathrm{u}_K^>)\rangle + \langle \mathrm{u}_K^< \cdot (\mathrm{u}_K^> \cdot \nabla \mathrm{u}_K^>)\rangle, \quad (8)$$

where $\mathrm{u}_K^<$ ($\mathrm{u}_K^>$) denotes the low-pass (high-pass) filtered velocities with respect to the cut-off wavenumber $K$, with $K^2 = k_x^2 + k_y^2$. The brackets $\langle\rangle$ denote a horizontal average over each subregion (see Scott and Wang 2005 for details about formula derivation). For these calculations, the upstream KE SSH field were partitioned into 12 overlapping boxes with 32×32 grid points, centered at 35°N, and every (1/3)° longitude between 142°E and 156°E (the gray boxes superimposed on Fig. 6). A Hanning window was applied to each box before taking DFT. The averaged $\Pi$ in each state was over all available weeks and all 12 boxes. A positive (negative) value of $\Pi$ indicates that the kinetic energy is trans-

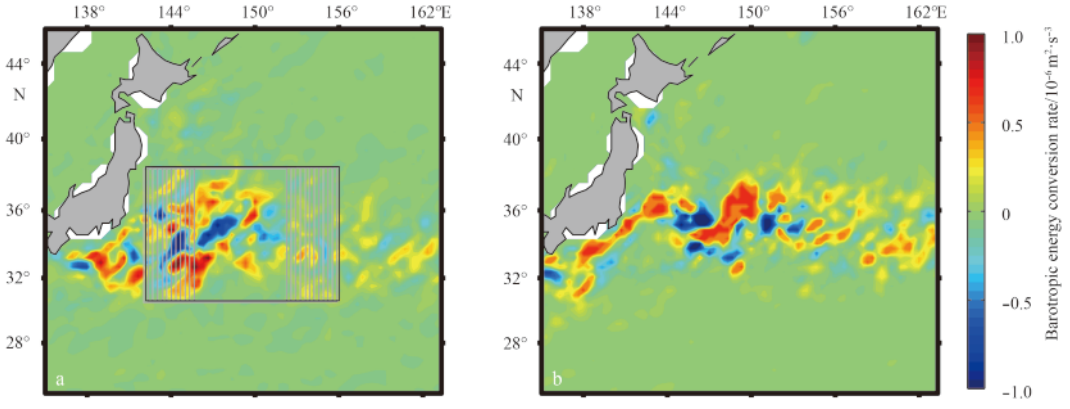


**Fig. 6.** Averaged spatial patterns of the barotropic energy conversion rate in unstable state (a) and stable state (b). The gray overlapping boxes superimposed on left panel denote homogeneous regions over which the spectral flux are computed in Section 3.4, and the whole region is identical to the region for HF-EKE in Fig. 1.

ferred from a small (large) wavenumber to a large (small) one, which implies a forward (inverse) cascade. The nonlinear terms tend to remove energy in the long-term mean at scales where $\prod$ has positive slope, which implies a power source to maintain a constant long-term mean spectral energy density.

In Fig. 7, the normalized spectral kinetic energy fluxes (solid curves) and the corresponding spectral kinetic energy densities (dash curves) in two states are depicted. The vertical solid lines denote the scales of maximum baroclinic instability at 35°N, 150°E (shown in Fig. 5), and the vertical dash lines denote the corresponding region-averaged Rossby deformation radius $L_{\mathrm{def}}$. It is clear in Fig. 7 that a large negative lobe of the spectral flux is significant in each state, which indicates an inverse cascade. By contrasting Fig. 7, it is found that the inverse cascade starts at scales about 300 km in the stable state, while there is a shift to small scales (about 270 km) in the unstable state. Meanwhile, the

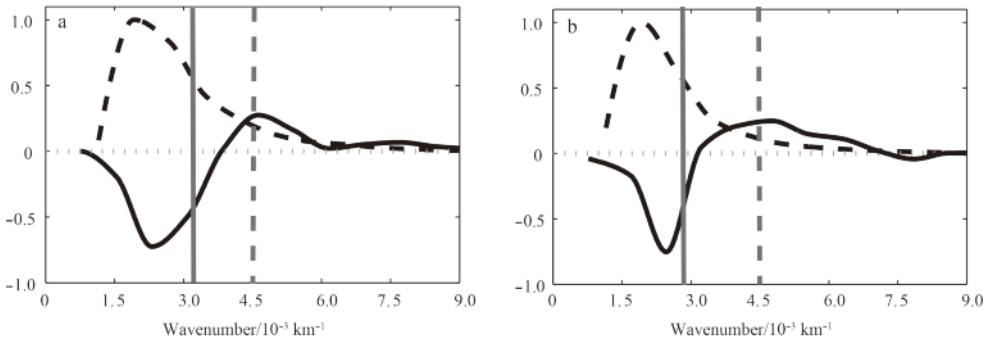


**Fig. 7.** Normalized spectral kinetic energy fluxes $\Pi$ (solid curves) plotted against total wavenumber ($10^{-3}$ cycles per kilometer) in the unstable state (a) and in the stable state (b), and the corresponding spectral kinetic energy densities (dash curves). The vertical solid lines denote the scales of maximum baroclinic instability at 35°N, 150°E, and the vertical dash lines denote the corresponding region-averaged Rossby deformation radius $L_{\mathrm{def}}$.

scale of the maximum baroclinic instability (solid vertical lines in Fig. 7) corresponds to the scales where $\prod$ has the almost steepest positive slope in both states, which is very likely to provide an evidence to support baroclinic instability as the mechanism deriving the inverse energy cascade in the upstream KE region.

The scale at which $\prod$ is minimum denotes the upscale kinetic energy begins to accumulate. Figure 7 shows that the upscale kinetic energy begins to accumulate from about 400 km in the stable state and 430 km in the unstable state. Meanwhile, the peak of the spectral kinetic energy density falls on the left shoulder of the inverse cascade in both states and is fairly consistent with the steepest negative slope in both states. All these results indicate that the observed eddy field in the upstream KE region is the result of an inverse cascade.

Finally, we discuss the interaction between eddy field and the mean flow in the spectral flux $\Pi$. To some extent, the mean flows could be considered as eddies with a wavenumber close to zero, i.e., $K \to 0$. So the barotropic instability would provide a positive contribution to $\Pi$, especially at large scales (small wavenumbers). Figure 7 shows that $\Pi$ has a shallower negative slope at small wavenumber in the unstable state than in the stable state which indicates that the barotropic instability is stronger in unstable state than in stable state. This seems fairly consistent with our results in Section 3.3.

Both the barotropic instability and baroclinic instability discussed above is under a local approximation. However, it is well-known that the fully-developed eddy field is not a local process. It also contains mesoscale signals propagating from the upstream and from the downstream. Meanwhile, the waves also contribute much to the SSHA signals. All these mesoscale signals interact with each other, and the kinetic energy transfers in the form of an inverse cascade to maintain the statistical stable spectral kinetic energy density. However, a full assessment of how much the advection of the mesoscale signals and waves account for the inverse cascade is beyond the scope of the present study.

## 4 Summary and discussion

This study has investigated the decadally modulating mesoscale eddy field in the upstream KE region, which has demonstrated that the HF-EKE (<300 d) level in the upstream region correlates well with the decadal KE path variability. The HF-EKE level is high (low) when the KE path is unstable (stable). Meanwhile, the energy-containing scale of the HF-EKE exhibits a good linear correlation with the HF-EKE, and the correlation coefficient is up to 0.85 after the seasonal variations are removed. Moreover, the mesoscale eddies in the upstream KE region are significantly zonally elongated in the unstable state, and a little meridionally elongated in the stable state. The linear baroclinic instability preferentially generates meridionally elongated eddies (Qiu et al., 2008, also proved in Fig. 6 in this paper), so the significantly zonally elongated eddies in the unstable state supports the possibility that the nonlinear transfer, via triad eddy interaction, works more effectively to redistribute EKE into zonally elongated eddies than that in the stable state.

In order to understand the mechanism dominating of the discovered phenomena, the local linear baroclinic instability and nonlinear eddy-mean flow interaction are examined in two different states. The results show that there is a more steeply sloping density structure (containing more APE) in the stable state than in the unstable state. Meanwhile, the local baroclinic growth rates, and scales of maximum instability are larger in the stable state than in the unstable state, which suggest that the local baroclinic instability is stronger in the stable state. Since the EKE level is lower in the stable state than in the unstable state, obviously the local linear baroclinic instability is not the dominant mechanism controlling the decadal modulation of the mesoscale eddy

field in the upstream region. On the other hand, the eddy field extracts more kinetic energy from the mean flows in the unstable state than in the stable state, which makes a positive contribution to the decadal modulation of the mesoscale field. However, it is worth noting that we are unable to conclude that the nonlinear barotropic instability is the dominant mechanism controlling the decadal modulation. The reason is that it is still not very clear whether there is advection of mesoscale signals, the waves and the wave-eddy interaction in different states, which make it is difficult to do the quantitive comparison.

The nonlinear eddy-eddy interactions were also investigated in this paper. The results showed that there were inverse kinetic energy cascades at scales larger than the Rossby deformation radius in both states. The inverse cascades start at scales being consistent with linear theory predicted the maximum baroclinic instability scales, which suggests that baroclinic instability may be one of the mechanisms driving the inverse cascade in both states. Meanwhile, the peak of the spectral kinetic energy density at scale which is fairly consistent with the steepest negative slope in both states, so the observed eddy field is the result of an inverse cascade, and cannot be explained by linear theory alone.

By comparing the inverse cascades in different states, it is found that the scale at which the inverse cascade starts is larger in stable state than that in unstable state. This finding is closely consistent with the theory that characteristic spatial scale of the linear baroclinic instability is larger in the stable state than in unstable state, which provides evidence that the inverse cascade of baroclinic kinetic energy is forced by baroclinic instability, even in the unstable state.

It is worth noting that the mesoscale signals appearing in the nonlinear spectral kinetic energy fluxes not only contain the eddies generated locally, but also contains the isolated warm- or cold- core eddies propagated from the east, because some of ocean eddies are observed to propagate westwards at speeds similar to the phase speeds of classical Rossby waves (Chelton et al., 2011). However, it is beyond the scope of the present study to investigate what extent the eddies propagating from the upstream and downstream account for the decadal modulation of the mesoscale eddy field in the upstream KE region.

***Acknowledgement***

We thank Rob Scott for his help in spectral flux calculation, and Qiu Bo for providing helpful feedback on interpreting altimeter data.

**References**

Arbic B K, Flierl G R. 2004. Effects of mean flow direction on energy, isotropy, and coherence of baroclinically unstable beta-plane geostrophic turbulence. Journal of Physical Oceanography, 34(1): 77–93

Berloff P, Meacham S P. 1998. On the stability of the wind-driven circulation. Journal of Marine Research, 56(5): 937–993

Bessières L, Rio M H, Dufau C, et al. 2013. Ocean state indicators from MyOcean altimeter products. Ocean Science, 9(3): 545–560

Charney J G, Stern M E. 1962. On the stability of internal baroclinic jets in a rotating atmosphere. Journal of the Atmospheric Sciences, 19(2): 159–172

Chelton D B, Schlax M G, Samelson R M. 2011. Global observations of nonlinear mesoscale eddies. Progress in Oceanography, 91(2): 167–216

Dewar W K, Bane J M. 1989. Gulf stream dynamics. Pad Ⅱ: eddy energetics at 73°W. Journal of Physical Oceanography, 19(10): 1574–1587

Dijkstra H A, Ghil M. 2005. Low-frequency variability of the large-scale ocean circulation: a dynamical systems approach. Reviews of Geophysics, 43(3): doi: 10.1029/2002RG000122

Ducet N, Le Traon P Y, Reverdin G. 2000. Global high-resolution mapping of ocean circulation from TOPEX/Poseidon and ERS-1 and -2. Journal of Geophysical Research: Oceans (1978–2012), 105(C8): 19477–19498

Eady E T. 1949. Long waves and cyclone waves. Tellus A, 1(3): 33–52

Ferrari R, Wunsch C. 2008. Ocean circulation kinetic energy: reservoirs, sources, and sinks. Annual Review of Fluid Mechanics, 41(1): 253–282

Frisch U. 1995. Turbulence: The Legacy of A.N. Kolmogorov. Cambridge: Cambridge University Press

Ingleby B, Huddleston M. 2007. Quality control of ocean temperature and salinity profiles-Historical and real-time data. Journal of Marine Systems, 65(1): 158–175

Jackett D R, McDougall T J. 1997. A neutral density variable for the world's oceans. Journal of Physical Oceanography, 27(2): 237–263

Kobashi F, Kawamura H. 2002. Seasonal variation and instability nature of the North Pacific Subtropical Countercurrent and the Hawaiian Lee Countercurrent. Journal of Geophysical Research: Oceans (1978–2012), 107(C11): 6–1–6–18

Le Traon P Y, Dibarboure G, Ducet N. 2001. Use of a high-resolution model to analyze the mapping capabilities of multiple-altimeter missions. Journal of Atmospheric and Oceanic Technology, 18(7): 1277–1288

Le Traon P Y, Nadal F, Ducet N. 1998. An improved mapping method of multisatellite altimeter data. Journal of Atmospheric and Oceanic Technology, 15(2): 522–534

Nonaka M, Xie Shangping. 2003. Covariations of sea surface temperature and wind over the Kuroshio and its extension: evidence for ocean-to-atmosphere feedback. Journal of Climate, 16(9): 1404–1413

Pedlosky J. 1964. The stability of currents in the atmosphere and the ocean: part I. Journal of the Atmospheric Sciences, 21(2): 201–219

Phillips N A. 1954. Energy Transformations and Meridional Circulations associated with simple Baroclinic Waves in a two-level, Quasi-geostrophic Model. Tellus A, 6(3): 273–286

Pierini S. 2006. A Kuroshio Extension system model study: decadal chaotic self-sustained oscillations. Journal of Physical Oceanography, 36(8): 1605–1625

Qiu Bo. 2002. The Kuroshio Extension system: its large-scale variability and role in the midlatitude ocean-atmosphere interaction. Journal of Oceanography, 58(1): 57–75

Qiu Bo, Chen Shuiming. 2005. Variability of the Kuroshio Extension jet, recirculation gyre, and mesoscale eddies on decadal time scales. Journal of Physical Oceanography, 35(11): 2090–2103

Qiu Bo, Chen Shuiming. 2006. Decadal variability in the formation of the North Pacific Subtropical Mode Water: oceanic versus atmospheric control. Journal of Physical Oceanography, 36(7): 1365–1380

Qiu Bo, Chen Shuiming. 2010. Eddy-mean flow interaction in the decadally modulating Kuroshio Extension system. Deep Sea Research Part Ⅱ: Topical Studies in Oceanography, 57(13–14): 1098–1110

Qiu Bo, Kelly K A. 1993. Upper-ocean heat balance in the Kuroshio Extension region. Journal of Physical Oceanography, 23(9): 2027–2041

Qiu Bo, Scott R B, Chen Shuiming. 2008. Length scales of eddy generation and nonlinear evolution of the seasonally modulated South Pacific Subtropical Countercurrent. Journal of Physical Oceanography, 38(7): 1515–1528

Scott R B, Wang Faming. 2005. Direct evidence of an oceanic inverse kinetic energy cascade from satellite altimetry. Journal of Physical Oceanography, 35(9): 1650–1666

Smith K S. 2007. The geography of linear baroclinic instability in Earth's oceans. Journal of Marine Research, 65(5): 655–683

Taguchi B, Xie Shangping, Schneider N, et al. 2007. Decadal variability of the Kuroshio Extension: observations and an eddy-resolving model hindcast. Journal of Climate, 20(11): 2357–2377

Tai C K, White W B. 1990. Eddy variability in the Kuroshio Extension

as revealed by Geosat altimetry: energy propagation away from the jet, Reynolds stress, and seasonal cycle. Journal of Physical Oceanography, 20(11): 1761–1777

Tulloch R, Marshall J, Hill C, et al. 2011. Scales, growth rates, and spectral fluxes of baroclinic instability in the ocean. Journal of Physical Oceanography, 41(6): 1057–1076

Tulloch R, Marshall J, Smith K S. 2009. Interpretation of the propagation of surface altimetric observations in terms of planetary waves and geostrophic turbulence. Journal of Geophysical Research: Oceans, 114(C2): doi: 10.1029/2008JC005055

Vivier F, Kelly K A, Thompson L A. 2002. Heat budget in the Kuroshio extension region: 1993–99. Journal of Physical Oceanography, 32(12): 3436–3454

Wang Shihong, Liu Zhiliang, Pang Chongguang. 2015. Geographical distribution and anisotropy of the inverse kinetic energy cascade, and its role in the eddy equilibrium processes. Journal of Geophysical Research: Oceans, 120(7): 4891–4906, doi: 10.1002/014JC010476

Waterman S, Hogg N G, Jayne S R. 2011. Eddy-mean flow interaction in the Kuroshio extension region. Journal of Physical Oceanography, 41(6): 1182–1208